International Journal of
Advances in Scientific Research and Engineering (ijasre)

E-ISSN : 2454-8006

DOI: 10.31695/IJASRE.2020.33938

Volume 6, Issue 12
December - 2020

The Use of *Citrullus Lanatus* for Corrosion Inhibition of A36 Steel in a CO_2 Saturated Saline Solution: A Thermodynamic and Kinetic Model Approach

Afoegba Clement . S[1]., Agbonkhese, Kingsley A[2]., Ohwojeheri, Abigail[3]

[1]Department of Welding Engineering and Offshore technology, Petroleum Training Institute (PTI), Efurun, Delta State, Nigeria

[2]Department of Mechanical Engineering Technology, National Institute of Construction Technology and Management (NICTM), Uromi, Edo State, Nigeria

[3]Department of Wet Chemistry, Thermo steel Nigeria Limited (Analytical/ Environmental Laboratory), Enerhen Road, Efurun, Delta State, Nigeria

ABSTRACT

Citrullus lanatus was tested for its suitability as an Inhibitor on Mild Carbon Steel in a Carbon (IV) Oxide (CO2) saturated saline solution. The mechanism of corrosion was investigated with and without Inhibitor additive in order to compare the effectiveness of the Inhibitor. Thermodynamic computations namely Enthalpy, Entropy and Gibbs free energy were used to determine the Inhibitive property of the Citrullus lanatus Extract. In addition, four Kinetic Models namely; Langmuir, Temkin, Flory-Huggins and Frumkin were also used to fit the experimental data. Gas Chromatography Mass Spectroscopy and Fourier Transfer Infrared Spectroscopy were used to characterize the Watermelon Seed Extract. Analysis of the results shows that Inhibitor efficiency decreases with increasing Temperature. The result also shows Inhibition efficiency within the range of 17.39%-71.79%. From the Result, the test sample without Inhibitor has the least Activation Energy in comparison with those with Inhibitor additives. The investigation also revealed that the Frumkin model at 50oC best fits the Experimental data with a Coefficient of determination, R2 of 99.9%, though; the other Models also fit the Experimental data.

Key Words: Corrosion, Citrullus Lanatus, Saline, Steel , Thermodynamic Model and Kinetic model.

1.0 INTRODUCTION

Daily Activities at the Industrial Environment from Exploration to Transportation ensures that there are movements of Industrial goods in an Environment that has Corrosion inducing properties due to the complex mixture of substances such as; Water, Mineral Acids, Oxygen, Carbon (IV) Oxide, Hydrogen Sulphide etc. (Singh et al., 2013).

It is therefore necessary for these Industrial goods to be transported around with Materials that have high corrosion resistance. Carbon Steel are widely used for the construction of Pipelines and other Equipment that is being used for production and Transportation of Industrial goods such as; Oil, Gas, Chemicals etc. Carbon Steel is considered as good alternative in this regard because of their relative cost and availability in comparison with Expensive Alloys. Notwithstanding, Carbon Steel are easily prone to corrosion attack because of their low resistance to corrosion (Fang et al., n.d.)

Several factors such as; pH, Temperature, Time etc. also affect the Corrosion behaviour of Carbon Steel.

The dangers associated with Corrosion could be Loss of Industrial goods through leakages, accident and eventually loss of revenues (Chesnokova et al., 2016). Due to the associated problems with corrosion, Industries mostly spend large percentage of their maintenance budget on Corrosion prevention and control (Bashir, et al., 2017 : Hassan et al., 2016; Tasić et al., 2018).

In order to successfully carryout effective corrosion prevention control on Carbon Steel, it is necessary to select Corrosion Inhibitors that are cost effective, environmentally friendly and easily available.

This study aims to investigate the Inhibitive properties of *Citrullus lanatus* seed extract on A36 Carbon Steel in a CO_2 saturated saline solution from a Thermodynamic and Kinetic Model approach.

(Go et al., 2020) also have shown that Iron Carbonate ($FeCO_3$) precipitation kinetics is extremely temperature-sensitive. At low temperatures (< 60^{o}C) Iron Carbonate does not adhere to the surface and is transported away from the surface by fluid movement.

2.0 EXPERIMENTAL

2.1 Materials and Solution

The specification of Carbon Steel used was ASTM A36 Carbon Steel. The A36 Carbon Steel has the following chemical composition;

Table 2.1: Chemical composition of the ASTM A36 Carbon Steel

Element Symbol	Element Name	Atomic Conc.	Weight Conc.
Fe	Iron	80.38	85.10
Ru	Ruthenium	1.33	2.55
Cl	Chlorine	3.21	2.16
Nb	Niobium	0.90	1.59
Ag	Silver	0.77	1.57
Si	Silicon	2.06	1.10
Ca	Calcium	1.26	0.96
Na	Sodium	2.05	0.89
K	Potassium	1.20	0.89
S	Sulphur	1.37	0.83
Mg	Magnesium	1.58	0.73
Al	Aluminium	1.22	0.62
P	Phosphorus	1.01	0.60
C	Carbon	1.09	0.25
O	Oxygen	0.58	0.17

Coupons of size 20mmx40mmx2mm were produced from the A36 Carbon Steel by cutting out the stated size. The Coupons were thoroughly cleaned with distil water and Acetone prior to setting up the experiment.

Citrullus lanatus (Watermelon) seed was purchased from the Local Market in Warri, Delta State, Nigeria. It was washed with water to remove debris and oven dried at mild temperature (50^{o}C) to reduce water content and not to destroy the phytochemical properties. The dried seeds were grounded with a mechanical grinder to increase the surface area and then, it was subject to solvent extraction with a Soxhlet apparatus using n-hexane as the extraction solvent.

A 3.5wt% of Sodium Chloride, NaCl solution was prepared by dissolving 3.5g analytical grade sodium chloride in a 100ml standard volumetric flask using distilled water. This solution was saturated by bubbling CO_2 gas through it at a constant rate after it has been deoxygenated. The solution was saturated with CO_2 gas when the pH became constant at 3.5.

2.2 EQUIPMENT

The apparatus used includes, dry oven, Soxhlet apparatus, gas cylinder, beaker, hot water bath, measuring cylinder, analytical weighing balance, and freeze dryer.

DOI: 10.31695/IJASRE.2020.33938

2.3 WEIGHT LOSS MEASUREMENT

Weight Loss Experiment was conducted by inserting the 20mmx40mmx2mm A36 Carbon Steel Coupon in the 3.5wt% NaCl solution that has been saturated with CO_2 gas. The experiment was conducted with (50ppm, 100ppm, 150ppm and 200ppm) and without the green Inhibitor in order to ascertain the effectiveness of the Inhibitor. The experiment was also investigated at different set temperature namely 40^{o}C, 50^{o}C, 60^{o}C, 70^{o}C and 80^{o}C in order to investigate the effect of Temperature on the Inhibitive property of the *Citrullus lanatus* Extract. Parameters such as Corrosion rate, Inhibition efficiency and Weight Loss were computed. The effect of the varying Inhibitor concentration was also investigated.

2.4 Thermodynamic Study

It is a well-known fact that the effect of temperature is highly complex but it provides the possibility of calculating the thermodynamic adsorption and kinetic corrosion parameters, which helps in determining the type of adsorption of the studied inhibitor as earlier reported by (Chakravarthy and Mohana, 2014). Different pH was also tested in order to compare the effect of pH on the Inhibition property of the *Citrullus lanatus* Seed Extract.

Activation Energy is a very important factor to consider when conducting Corrosion experiment and this is because for corrosion to occur, the minimum activation energy of the medium has to be overcome (Oguntade et al., 2020). The Activation Energy was calculated using the Computational Equation below;

$$\text{Log CR} = \frac{-E_a}{2.303RT} + \log A \qquad 2.1$$

Where;

E_a =The activation energy of the reaction

R =The universal gas constant (8.314 J/mol)

CR =The corrosion rate

T = Temperature

In addition, The Enthalpy and Entropy of the system was also calculated in order to ascertain the nature of the corrosion reaction and the degree of disorderliness of the system. The Enthalpy and Entropy were calculated using the relationship below;

$$\log\left(\frac{CR}{T}\right) = \log\left(\frac{R}{N_h}\right) + \frac{\Delta S_{ads}}{2.303R} - \frac{\Delta H_{ads}}{2.303T} \qquad (2.2)$$

Where;

N =Avogadro's Number (6.02252 x 10^{23} mol^{-1})

R =The universal gas constant (8.314 J/mol)

h = Plank's constant (6.626176 x 10^{34}Js)

T = Temperature

(ΔH_{ads}) = Enthalpy of the system

(ΔS_{ads}) = Entropy of the system

2.5 Adsorption Isotherm

Langmuir, Temkin, Flory Huggins and Frumkin Adsorption Isotherm were utilized for this study in order to investigate the nature of the Adsorption in the Corrosion process and also to investigate the Models that closely fit the Experimental Data.

The Langmuir Adsorption Isotherm was determined using the equation below;

$$\frac{C}{\emptyset} = K+C \qquad (2.3)$$

DOI: 10.31695/IJASRE.2020.33938

Where;

C =Inhibitor concentration

∅=Degree of surface covered by the inhibitor

K =Adsorption equilibrium constant

The Temkin isotherm is given by

$$\emptyset = -2.303 \log K/2a - 2.303 \log C/2a \quad (2.4)$$

Where, C is the inhibitor concentration, ∅ is the degree of surface covered by the inhibitor, K is the adsorption equilibrium constant and a is the attractive parameter.

The Flory-Huggins isotherm is given by

$$\text{Log } (\emptyset/\mathbf{C}) = \log K + X \log (1 - \emptyset) \quad (2.5)$$

Where C is the inhibitor concentration, ∅ is the degree of surface covered by the inhibitor, K is the adsorption equilibrium constant and x is the size parameter.

The Frumkin isotherm is given by

$$\text{Log}(C * \emptyset\ 1-\emptyset) = 2.303 \log K + 2 \propto \emptyset \quad (2.6)$$

Where C is the inhibitor concentration, ∅ is the degree of surface covered by the inhibitor, K is the adsorption-desorption constant and ∝ describes the interaction in the adsorbed layer (lateral interaction term).

2.6 FTIR Analysis

Fourier Transfer Infrared Spectroscopy analysis was conducted in order to determine the functional groups that are present in the Inhibitor. This is also important in corroborating the Inhibitive property of the *Citrullus lanatus* seed Extract particularly in examining the type of bonding that will exist between the Inhibitor and the Metal surface (Donatus et al., 2017; Taheri et al., 2017; Veneranda et al., 2016).

3.0 RESULTS AND DISCUSSION

3.1 Weight Loss Measurement

Temperature is a dominant factor in determining the rate of Corrosion in a Carbon dioxide Saline solution due to its conflicting factor (Afolabi et al., 2020). Generally, at low pH, increase in Temperature increases the precipitation of Hydrogen Ion which is unfavourabe for the protective film covering but at high pH, increase in Temperature increases the formation, density and insolubility of the Iron Carbonate layer which provides the protective film covering on the metal surface (Durowaye et al., 2014)

Table 3.1: Corrosion Rate and Inhibitor Efficiency at Temperature 40^{o}C and pH 3.15

Concentration (mg/L)	Weight Loss	Corrosion Rate (mm/hr)	Inhibitor Efficiency (%)
0 (Control)	0.37	0.565	0
50	0.13	0.198	64.86
100	0.11	0.168	70.27
150	0.11	0.168	70.27
200	0.14	0.214	62.16

Table 3.1 represents the Corrosion rate and the Inhibitor (*Citrullus lanatus*) efficiency when the solution is fully saturated at a pH of 3.15 and using a set Temperature of 40^{o}C. From Table 3.1, the Corrosion rate decreases from 0.57mm/hr. to 0.21mm/hr with an Inhibitor concentration of 0mg/L (Control) and 200mg/L respectively. The reason for this, is because, the solution with Inhibitor helps to prevent the Solubility of Iron Carbonate on the surface of the Coupons due to the protective film covering that was provided by the Inhibitor in comparison to the solution without an Inhibitor (Control) (Abdullahi et al., 2020; Oloruntoba et al.,

DOI: 10.31695/IJASRE.2020.33938

2020; Oluyori et al., 2020). Observation similar to this was also reported by (Tariq Saeed et al., 2020). Furthermore, a closer observation of the result shows that there was a progressive decrease of Corrosion rate (0.198mm/hr to 0.168mm/hr) as the inhibitor concentration increases from 50mg/L to 100mg/L and almost became steady at 150mg/L, then, the corrosion rate increased when the Inhibitor Concentration was increased further to 200mg/L. Similar observation was also reported by (Oguntade et al., 2020) . This shows that when the Solution is fully saturated with CO_2 gas at a Temperature of 40^oC, Inhibitor concentration should not exceed 150mg/L in order to have an effective Corrosion control on the Carbon Steel since increasing the Inhibitor concentration further, will result in an increase in the Corrosion rate which is not suitable for design of process systems that can control the rate of Corrosion of Carbon Steel using *Citrullus lanatus* Seed Extract as the Inhibitor (Onyeachu et al., 2019). More so, this observation is clearly supported from the results of the Inhibitor efficiency. From Table 3.1, the Inhibitor efficiency increases from 0 (Control, without Inhibitor) to 64.86% (50mg/L Inhibitor Concentration) and almost became steady (70.27%) from 100mg/L to 150mg/L of Inhibitor Concentration and gradually decreased to 62.16% at Inhibitor Concentration of 200mg/L. Observation similar to those presented here was also reported by (Oyekunle et al., 2019).

Table 3.2: Weight Loss, Corrosion Rate and Inhibitor Efficiency at Temperature 50^oC and pH 3.15

Concentration (mg/L)	Weight Loss	Corrosion Rate (mm/hr)	Inhibitor Efficiency (%)
0 (Control)	0.39	0.59	0
50	0.23	0.35	41.02
100	0.18	0.27	53.85
150	0.14	0.21	64.1
200	0.11	0.17	71.79

The result for the Corrosion rate and Inhibitor efficiency at a pH of 3.15 and Temperature of 50^oC is shown in Table 3.2. The results show that Corrosion rate decrease was steady as Inhibitor Concentration increases. This observation is also supported by the Inhibitor efficiency trend from figure 4.5 which shows a steady increase as the Inhibitor Concentration increases (50mg/L, 100mg/L, 150mg/L, and 200mg/L). (Ibrahim et al., 2017) proposes that Corrosion rate decreases as Inhibitor concentration increases at a higher Temperature because as the Temperature increases to 50^oC, the reduction reaction which accelerates the rate of corrosion decrease in the medium, increases because the increased concentration of the Inhibitor provides more protective film covering which is necessary for corrosion control. Similar view was also investigated by (Fiori-Bimbi et al., 2015; Souza et al., 2020)

Table 3.3: Corrosion Rate and Inhibitor Efficiency at Temperature 60^oC and pH 3.15

Concentration (mg/L)	Weight Loss	Corrosion Rate (mm/hr)	Inhibitor Efficiency (%)
0 (Control)	0.42	0.64	0
50	0.27	0.41	35.71
100	0.24	0.36	42.86
150	0.15	0.23	64.29
200	0.16	0.24	61.9

The trend in Corrosion rate decrease and the Efficiency of the Inhibitor at a temperature of 60^oC when the solution was fully saturated with CO_2 at a pH of 3.15 is as shown in figure Table 3.3. The results (Table 3.3) show that there was a continuous decrease in Corrosion rate and continuous increase in the Inhibitor efficiency as the Inhibitor concentration increases. This shows that even though at a pH of 3.15 when the reduction of Hydrogen ion is supposed to be the rate controlling mechanism of the reaction, thus, causing an increase in the corrosion rate, the increase in Temperature to 60^oC, enables a faster precipitation of the corrosion protective film which further ensures that more protective films are being formed that spread across the coupon giving room for only localised corrosion to occur (Li et al., 2019; Rivera-Grau et al., 2012). This observation was supported by (Gunavathy and Murugavel, 2012) which suggested that more corrosion protective film is being precipitated in a solution with Inhibitor as temperature is being increased from 20^oC. A comparison of this observation with the Control solution without Inhibitor (0mg/L Inhibitor concentration) from figure 4.9 shows that the solution without an Inhibitor has the highest corrosion rate and this is because as the hydrogen ion concentration is dominant in the medium, there was no protection for the Coupon giving room for the corrosion product to attack the entire surface of the Coupon which further leads to a general corrosion taking place (Tasić et al., 2018) . Observation similar to this was also reported by (Palumbo et al., 2019).

DOI: 10.31695/IJASRE.2020.33938

Table 3.4: Corrosion Rate and Inhibitor Efficiency at Temperature 70°C and pH 3.15

Concentration (mg/L)	Weight Loss	Corrosion Rate (mm/hr)	Inhibitor Efficiency (%)
0 (Control)	0.23	0.34	0
50	0.19	0.28	17.39
100	0.19	0.28	17.39
150	0.15	0.23	34.78
200	0.11	0.17	24.83

The results for the variation of corrosion rate and the inhibitor efficiency with Inhibitor concentration is as presented in Table 3.4. The result shows an increasing trend of Inhibitor efficiency from Inhibitor concentration 0mg/L (Control) to Inhibitor concentration 100mg/L, with a slight decrease at Inhibitor concentration 150mg/L and a continuous increase at 200mg/L. The result also shows that the corrosion rate decreases from Inhibitor concentration 0mg/L (control) to 100mg/L with a slight increase at 150mg/L and a downward decrease at 200mg/L. The reason for slight changes of the Inhibitor behaviour at Concentration 150mg/L may be due to a slight desorption of the Inhibitor molecules on the surface of the carbon steel (Farhadian et al., 2020; Obot et al., 2019)

Table 3.5: Corrosion Rate and Inhibitor Efficiency at Temperature 80°C and pH 3.15

Concentration (mg/L)	Weight Loss	Corrosion Rate (mm/hr)	Inhibitor Efficiency (%)
0 (Control)	0.41	1.43	0
50	0.26	0.39	36.59
100	0.24	0.36	41.46
150	0.17	0.26	58.54
200	0.15	0.23	63.41

Table 3.5 shows a representation of the behaviour of the Inhibitor molecules in terms of the variation of the Inhibitor efficiency and the corrosion rate with Inhibitor concentration. The result shows that there was a continuous fluctuation of the Inhibitor efficiency and the Corrosion rate. The reason for this behaviour is because at temperature of 80°C, the rate of reaction will be very high (Rajendrachari, 2018; Salinas-Solano et al., 2018; Xu et al., 2017) in comparison with Temperature 40, 50, 60 and 70 and this is because the rate of reaction increases with temperature (Akhavan et al., 2018). Thus, at this high rate of reaction, the Inhibitor molecules will tend to adhere to the surface of the carbon steel faster but because of the acidity of the solution, there may also be a counter reaction of desorption of the inhibitor from the surface of the carbon steel as well due to the faster rate of reaction which then leads to instability of the protective film covering (Lgaz et al., 2017)

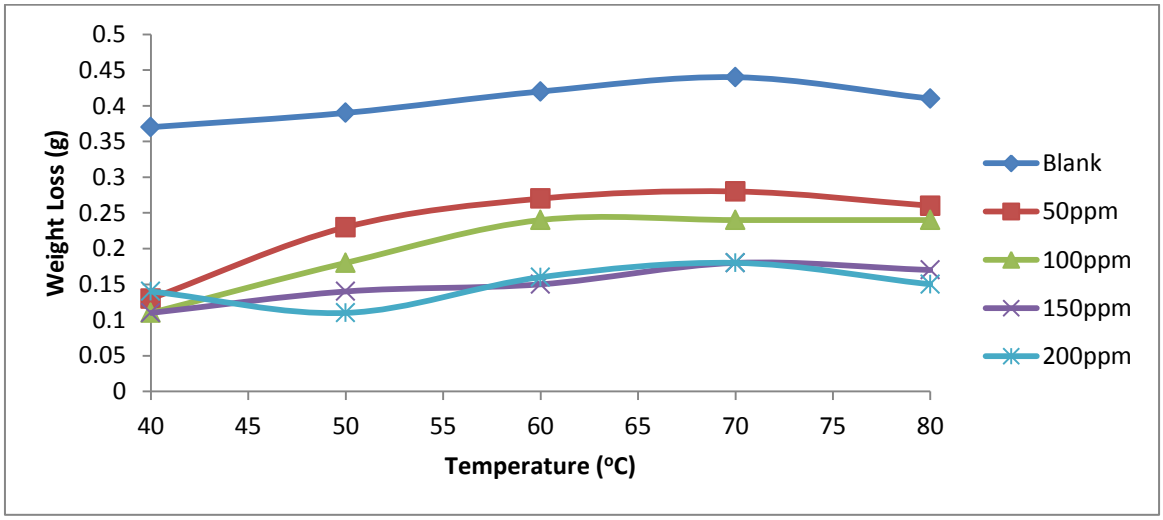

Figure 3.1: Variation of Weight Loss with Temperature at pH 3.15

DOI: 10.31695/IJASRE.2020.33938

Figure 3.1 represents the Weight Loss when the solution is fully saturated with CO_2 at a pH of 3.15 at varying Temperature of 40°C-80°C. From Figure 3.1, it can be observed that the Weight loss increases as the Temperature increased from 40-70 and decreases when the Temperature is 80°C for all the Inhibitor concentration (50mg/L-200mg/L) under consideration. The reason for the increase in weight loss behaviour may be due to the non-film forming condition (Han et al., 2018) at these temperature range (40°C-70°C) but there was a drop in weight loss when the temperature increased to 80°C as a result of the less difficulty in forming protective film at that condition as observed by (Go et al., 2019). In addition, it was observed that the Weight Loss decreases as the Inhibitor concentration increases from 0mg/L (Control) to 200mg/L respectively. The reason for this, is because, the solution with Inhibitor helps to prevent the Solubility of Iron Carbonate on the surface of the Coupons due to the protective film covering that was provided by the Inhibitor in comparison to the solution without an Inhibitor (Control). Observation similar to this was also reported by (Durowaye et al., 2014; Mamedaliev Institute of Petrochemical Processes, National Academy of Sciences of Azerbaijan, AZ1025 Baku, Azerbaijan et al., 2015; Pfennig et al., 2011; Sotelo-Mazon et al., 2020)

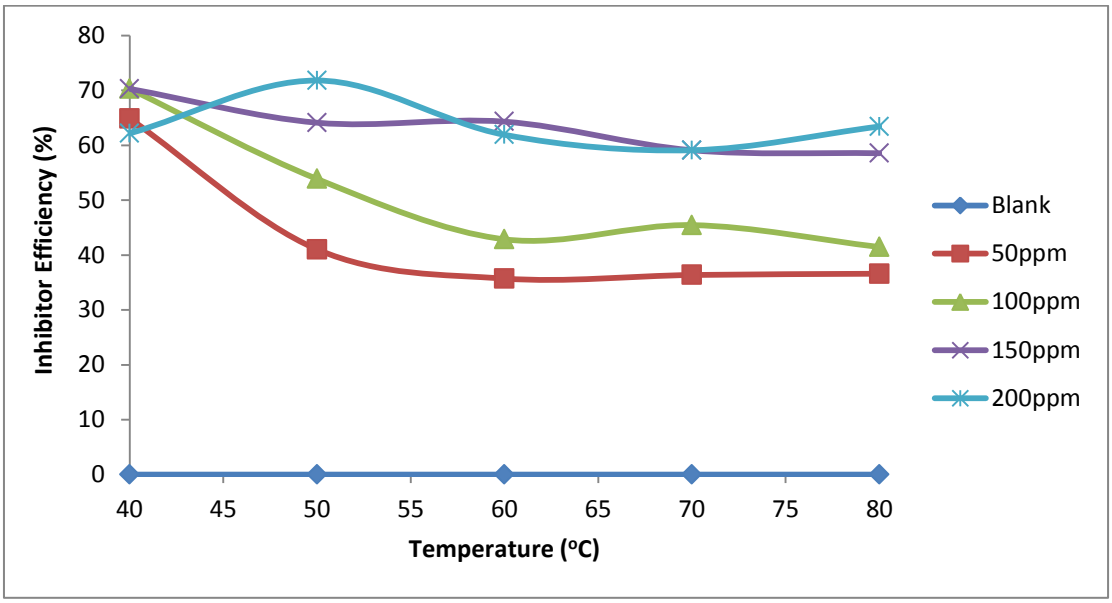

Figure 3.2: Variation of Inhibitor Efficiency with Temperature at a pH of 3.15

The Temperature can be said to have two conflicting effect. With a rise in Temperature, the Corrosion rate shows increase and decrease with respect to the solubility limit of Iron Carbonate Layer (Farhadian et al., 2020). At the non-film forming conditions (Low pH), increasing the Temperature results to an increase in the Corrosion rate and a decrease in the efficiency (Li et al., 2019). An observation of the results (Figure 3.2) show that the Efficiency of the Inhibitor increases with increase in Inhibitor Concentration for the same pH level. Notably from Figure 3.2, the efficiency increases from 0% to 71.79% as the Inhibitor concentration increases from 0ppm to 200ppm. Observation of the results also shows that as Temperature increases, Inhibitor Efficiency decreases.

3.2 Thermodynamic Study

Table 3.6: Kinetic data for half-life at pH 3.15

Concentration (ppm)	k	Half-life, t	R^2
Blank	0.117	5.923	83.94
50	0.127	5.457	98.25
100	0.144	4.812	93.07
150	0.155	4.471	88.65
200	0.189	3.667	81.86

The activation energy is the minimum amount of Energy that is required for a reaction to occur. Inhibitors act as negative catalyst, thus, increasing the activation Energy of the reaction and this helps to slow down the Corrosion rate (Akinbulumo et al., 2020). It was observed that generally, the Activation Energy increases with increasing Inhibitor concentration though there may be slight changes to this depending on whether desorption or adsorption is taking place at increasing Inhibitor concentration as observed in this study (Adesina et al., 2020).

DOI: 10.31695/IJASRE.2020.33938

Table 3.7 Activation Energy for pH 3.15

Concentration (ppm)	Ea (KJ/Mol)	R^2
Blank	4.03	76.33
50	12.65	95.37
100	8.67	84.33
150	12.35	87.62
200	13.75	97.32

The activation energy observed in Table 4.7 shows that the sample without Inhibitor additive (Blank) has the lowest Activation Energy (4.03KJ/Mol) compared with those with Inhibitor additives (50ppm, 100ppm, 150ppm and 200ppm) with respective Activation Energy as 12.65KJ/Mol, 8.67KJ/Mol, 12.35KJ/Mol and 13.75KJ/Mol. The reason for this was due to easier dissolution of the protective film covering on the Coupon without Inhibitor Additive (Cen et al., 2019) which in turn requires lesser energy for corrosion to occur in comparison with those that have Inhibitive Additives that helps to prevent the fast dissolution of the protective film covering (Ademoh, 2012) .

Table 3.8: Enthalpy and Entropy values at pH 3.15

Concentration (ppm)	ΔHa	ΔSa
Blank (0)	1813.66	132.17
50	1411.74	130.21
100	1710.02	130.94
150	924.82	137.36
200	339.83	126.55

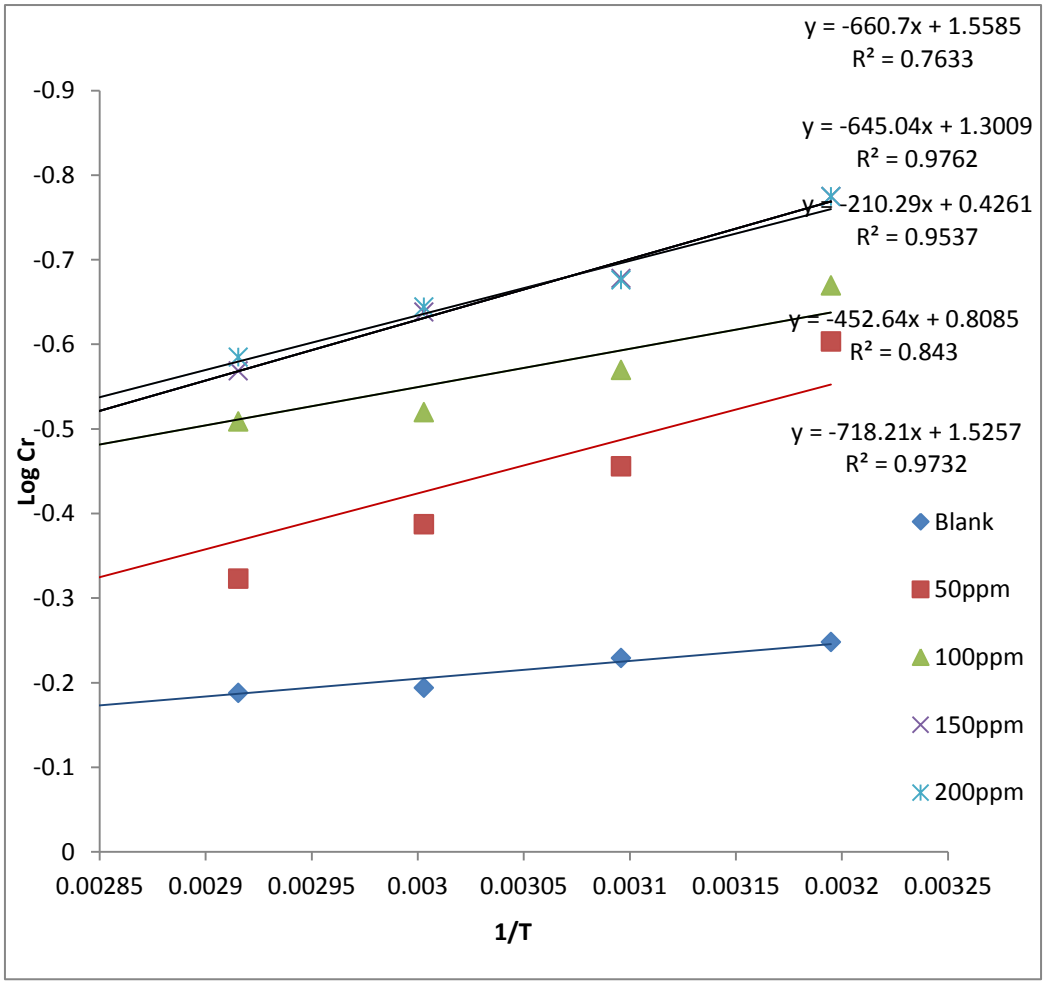

Figure 3.3:Arrhenius Plot for Activation Energy at pH 3.15

DOI: 10.31695/IJASRE.2020.33938

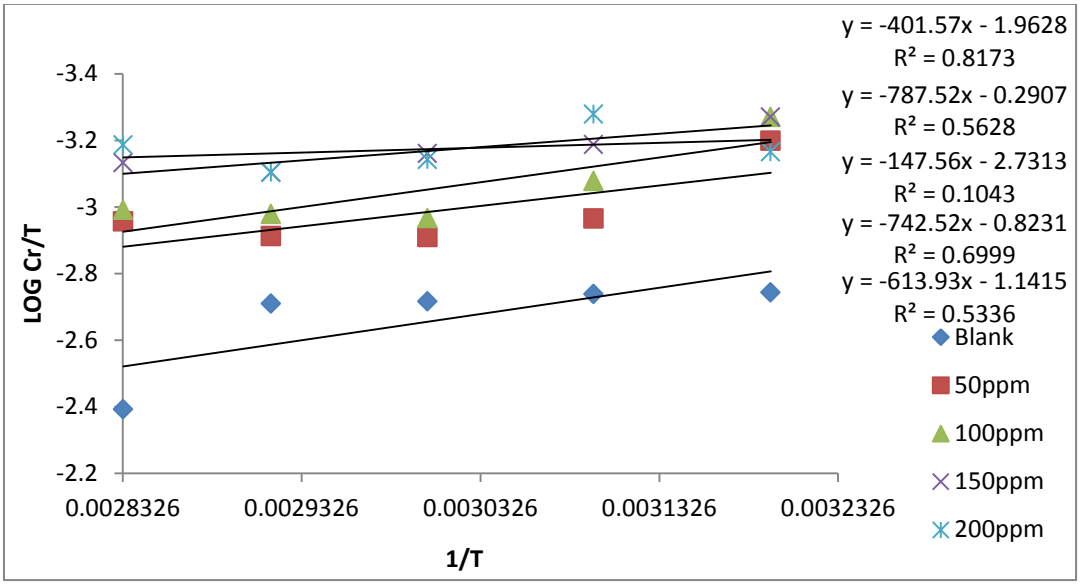

Figure 3.4:Plot of Log Cr/T versus Temperature at pH 3.15

3.2.1 Adsorption Isotherm

Table 3.9: Coefficient of determination, R^2 for the entire Adsorption Models

Temperature K	Langmuir R^2	Temkin R^2	Frumkin R^2	Flory-Huggins R^2
313	0.985	0.753	0.901	0.631
323	0.992	0.992	0.999	0.958
333	0.906	0.857	0.961	0.582
343	0.868	0.439	0.768	0.01
353	0.927	0.949	0.997	0.722

Adsorption isotherm for pH 3.15 and Temperature 40^{o}C

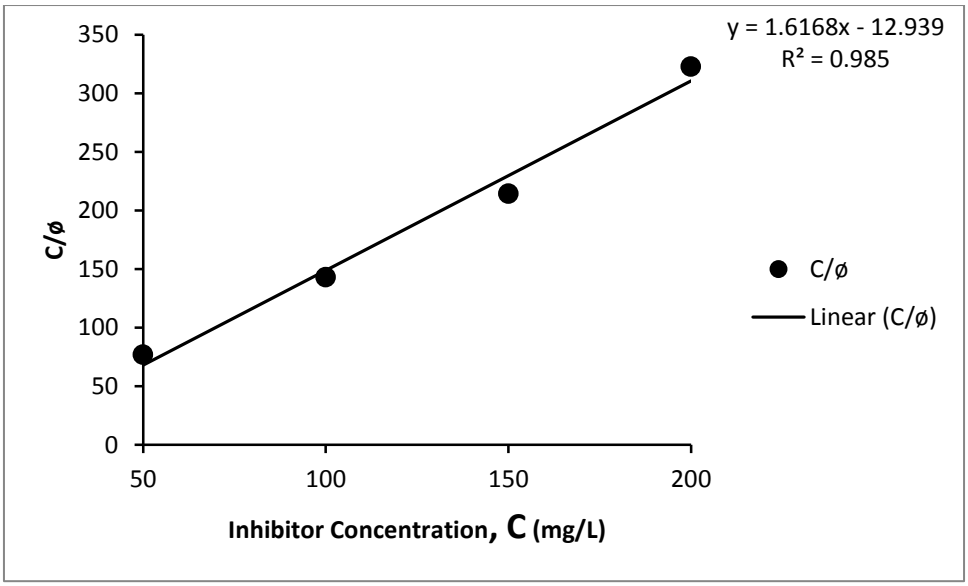

Figure 3.5: Langmuir model

DOI: 10.31695/IJASRE.2020.33938

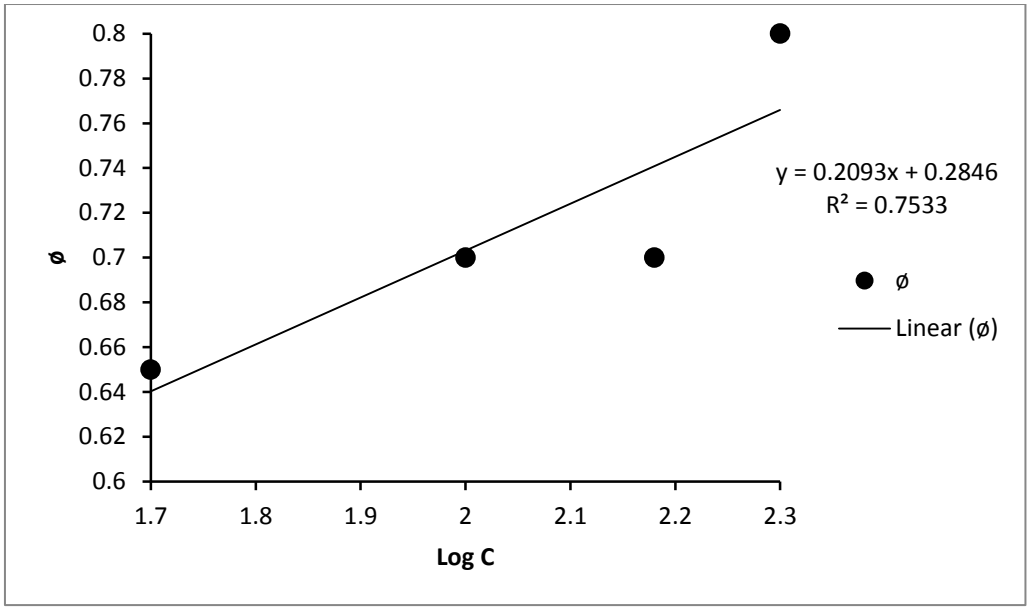

Figure 3.6: Temkin Model

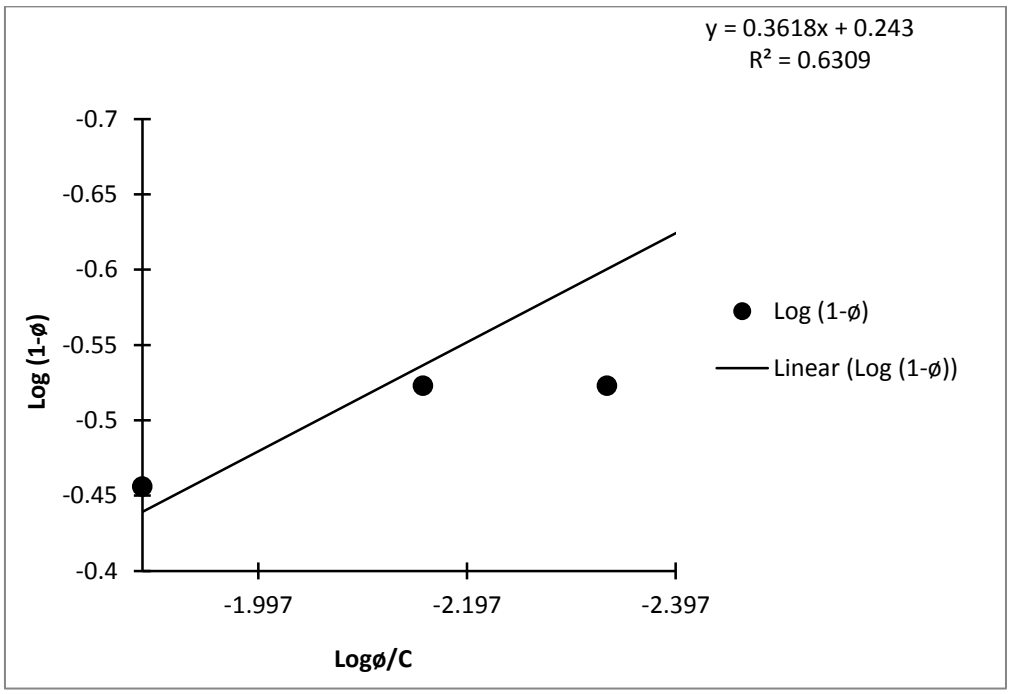

Figure 3.7: Flory-Huggins model

DOI: 10.31695/IJASRE.2020.33938

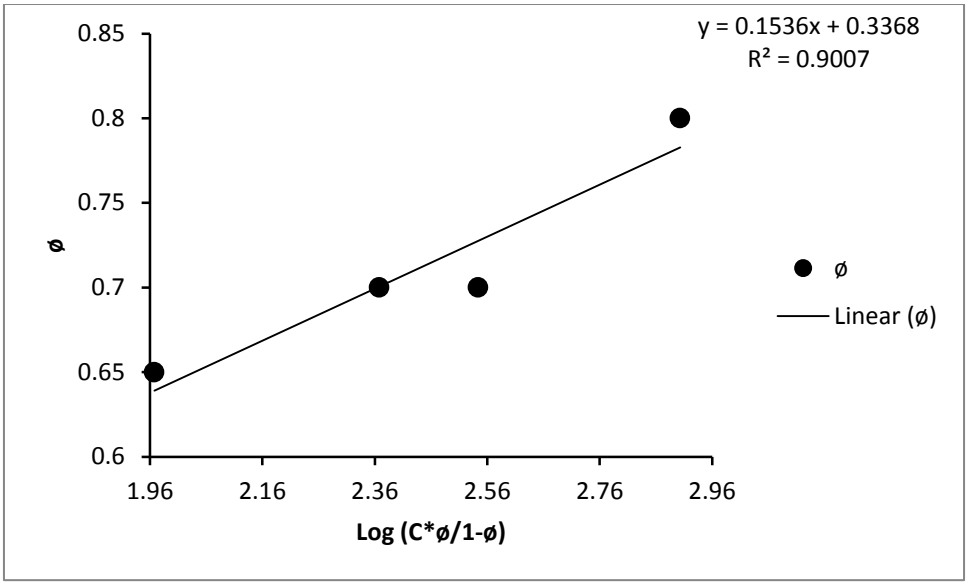

Figure 3.8: Frumkin Model

The adsorption isotherm for pH 3.15 and Temperature 40^{o}C is shown in Figures 4.21-4.24.

From figure 4.21, it can be seen that the Langmuir model closely fit the Experimental data of this study in comparison with the Temkins model (Figure 4.22), Flory-Huggins model (Figure 4.23) and Frumkin model (Figure 4.24). This is evidence from the high Coefficient of determination, R^2 value of 98.5% in the Langmuir model when compared with the Temkin, Fory-Huggins and Frumkin models which have a Coefficient of determination, R^2 value of 75.3%, 63.1% and 90.1% respectively.

Adsorption isotherm for pH 3.15 and Temperature 50^{o}C

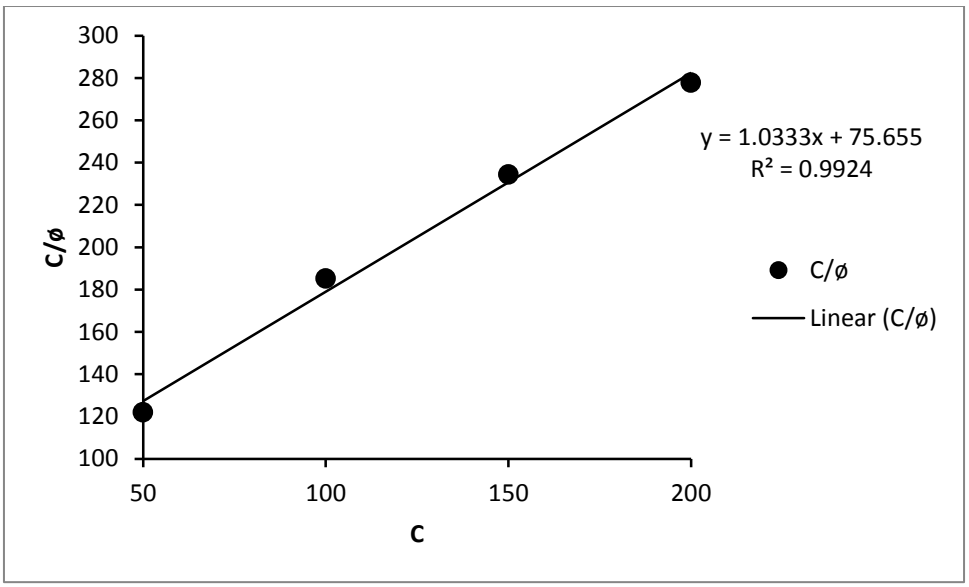

Figure 3.9: Langmuir model

DOI: 10.31695/IJASRE.2020.33938

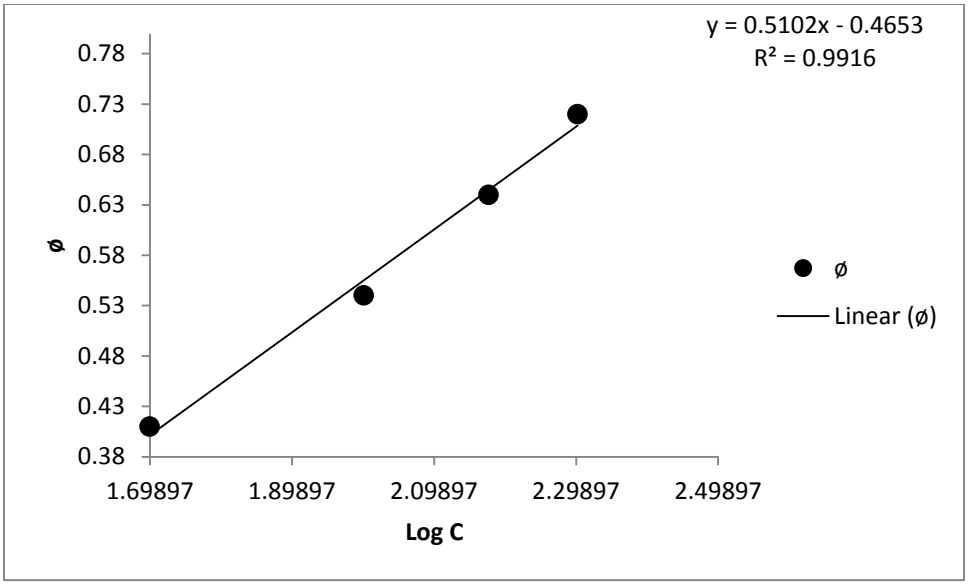

Figure 3.10: Temkin model

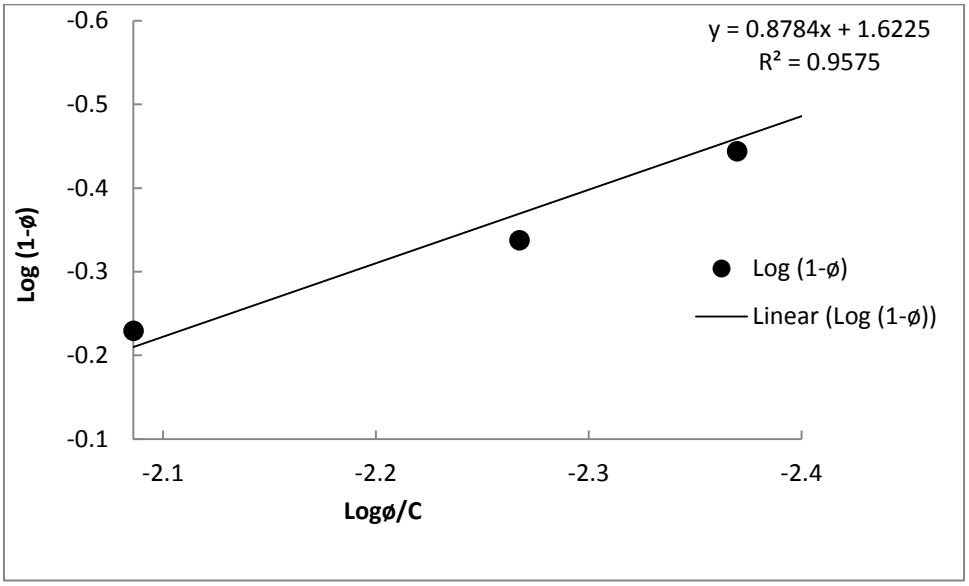

Figure 3.11: Flory-Huggins model

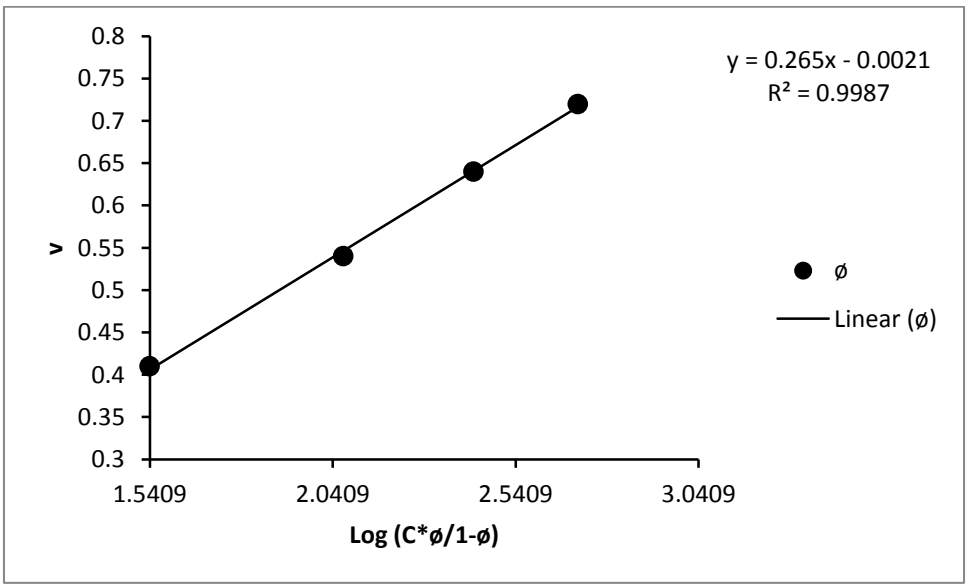

Figure 3.12: Frumkin Model

DOI: 10.31695/IJASRE.2020.33938

The results for the adsorption Isotherm are shown in figure 4.25 (Langmuir), 4.26 (Temkin), 4.27 (Flory-Huggins) and 4.28 (Frumkin)

The results show that the Experimental results agree to the entire adsorption isotherm but the Frumkin Isotherm with a Coefficient of determination value, R^2 of 99.9% (Figure 4.28) fits the experimental data better in comparison with the Langmuir (99.2%), Temkin (99.2%) and Flory-Huggins (95.8%). In addition, following the result of the Langmuir isotherm (Fig. 4.25), the slope (1.03) of the equation closely agrees with the prediction of Langmuir adsorption isotherm which stated that an equation with a slope of unity (1.0) is in a good agreement with the Langmuir model(Al-Haj-Ali et al., 2014; Go et al., 2020; Hribšek, n.d.; Loto, 2018; Xu et al., 2017)

Adsorption isotherm for pH 3.15 and Temperature 60^{o}C

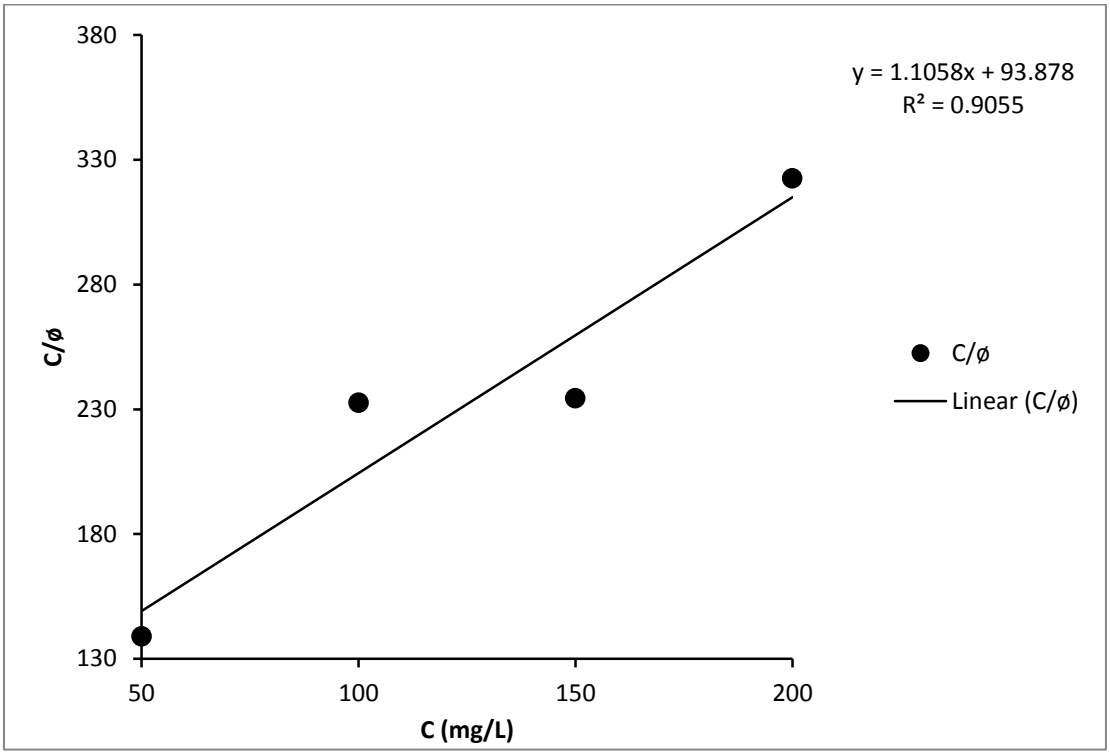

Figure 3.13: Langmuir model

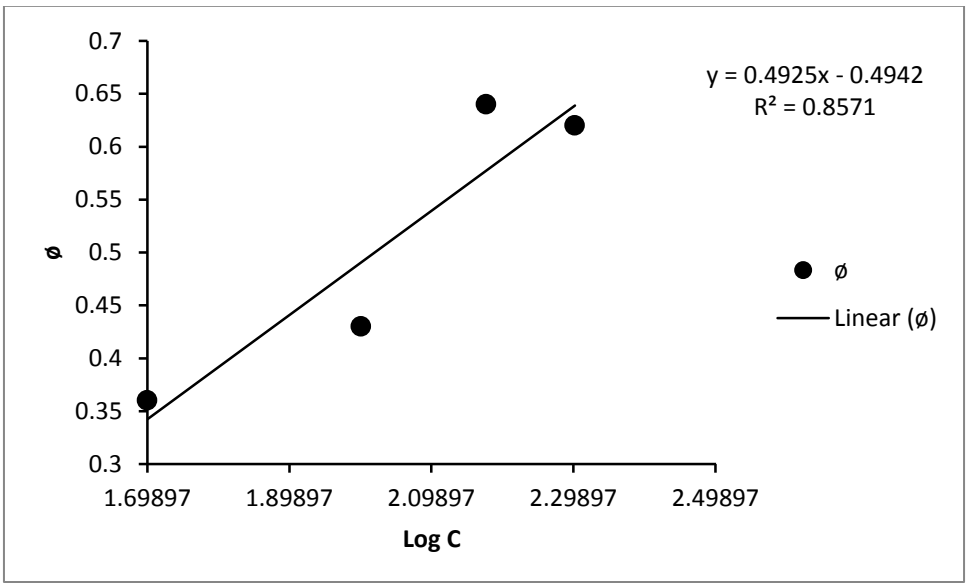

Figure 3.14: Temkin model

DOI: 10.31695/IJASRE.2020.33938

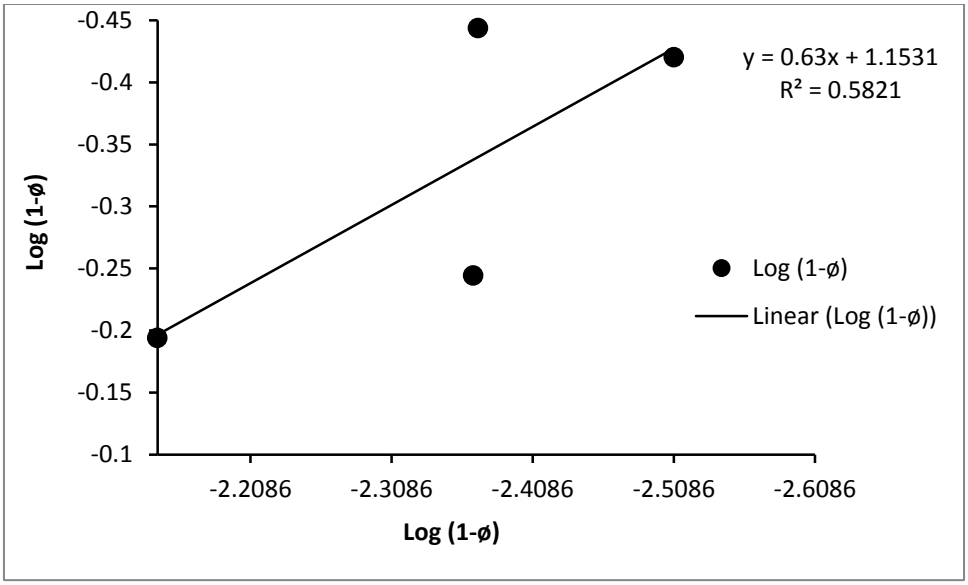

Figure 3.15: Flory-Huggins model

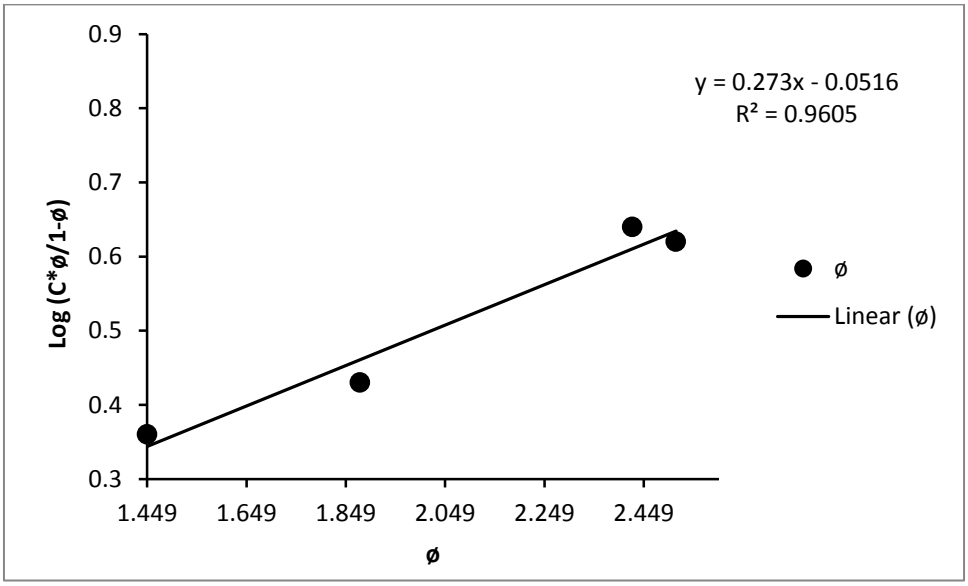

Figure 3.16: Frumkin Model

Figures 4.29-4.32 represents the Langmuir, Temkin, Flory-Huggins and Frumkin adsorption isotherm obtained from the experimental results at a Carbon(IV) Oxide (CO_2) saturated pH of 3.15 and a Temperature of 60^oC of this study. It can be observed that the Experimental result closely fits the Frumkin Adsorption Isotherm in comparison with the other adsorption Isotherms. From figure (4.31), the Experimental Results deviated from the Flory-Huggins adsorption Isotherm given its low value of Coefficient of determination (R^2) value of 58.2%.

Adsorption isotherm for pH 3.15 and Temperature 70^oC

DOI: 10.31695/IJASRE.2020.33938

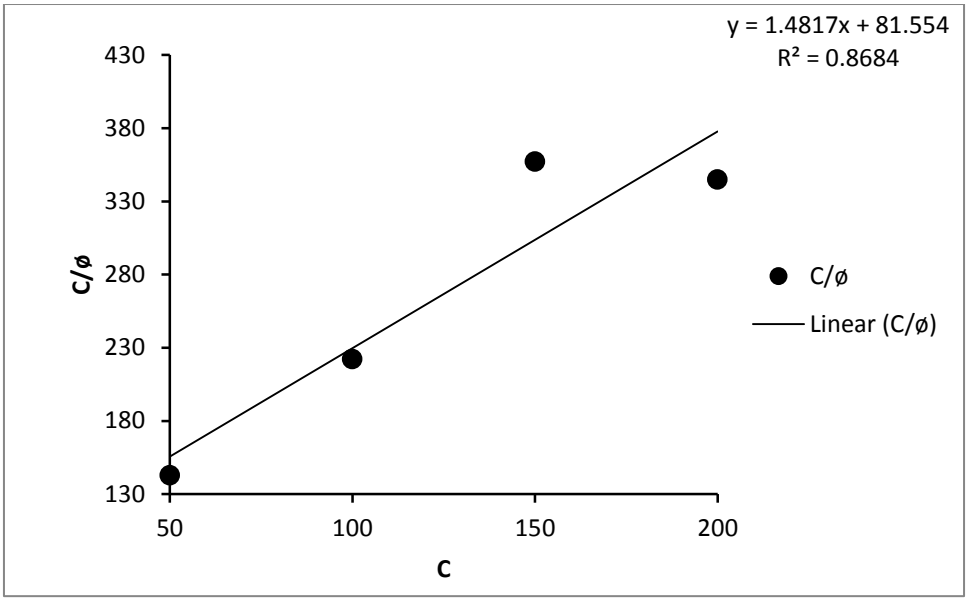

Figure 3.17: Langmuir model

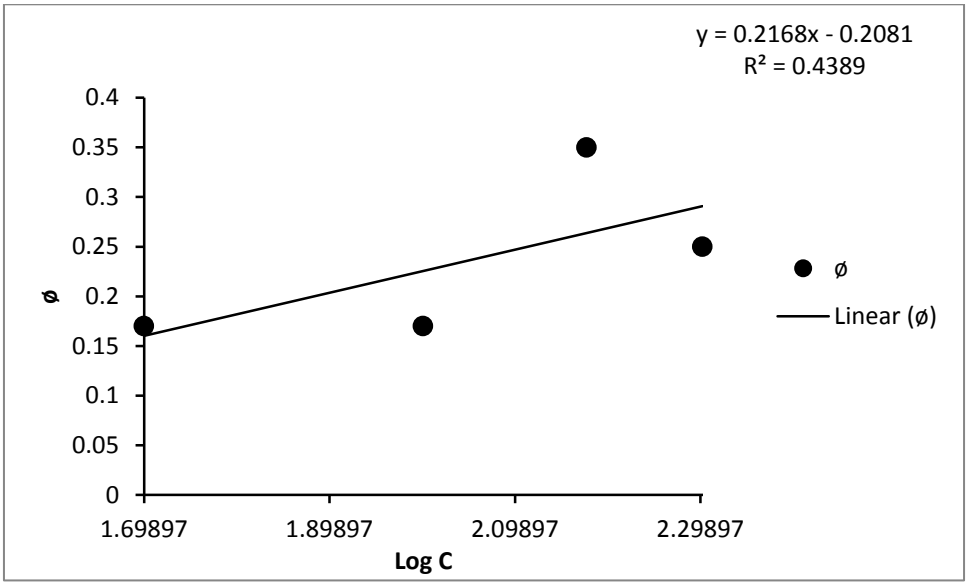

Figure 3.18: Temkin model

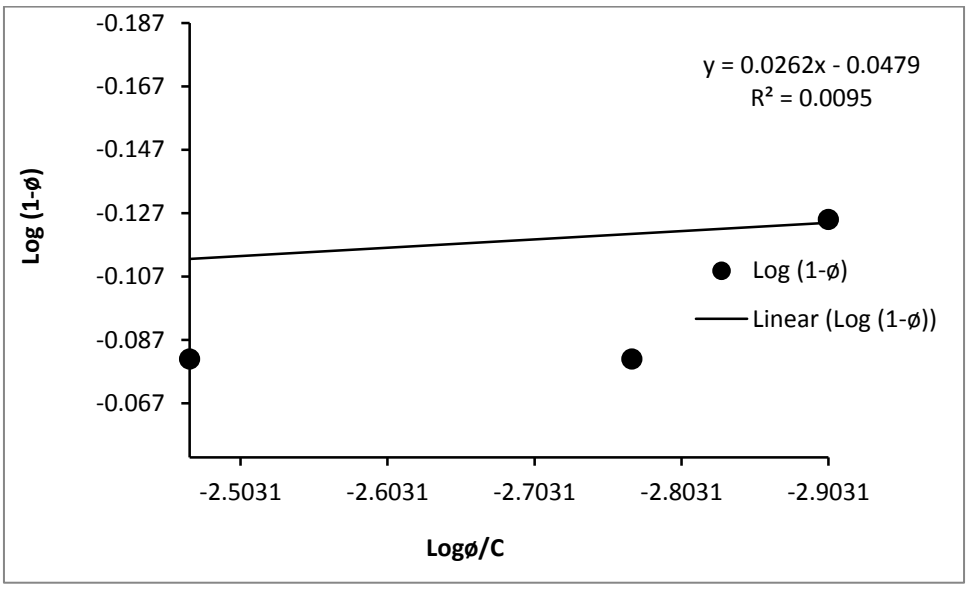

Figure 3.19: Flory-Huggins model

DOI: 10.31695/IJASRE.2020.33938

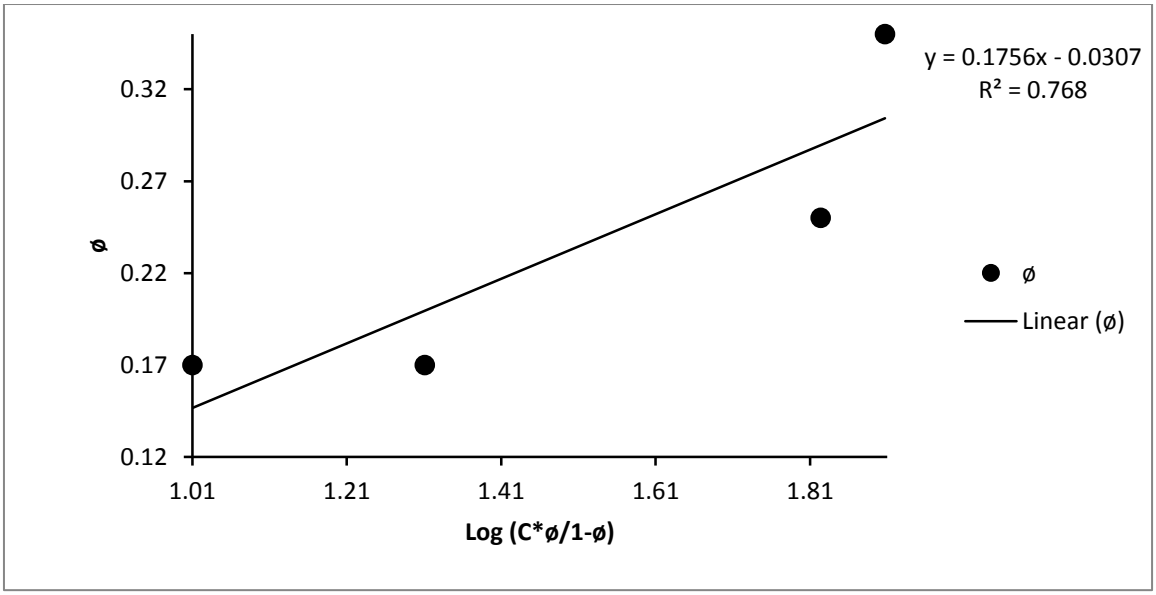

Figure 3.20: Frumkin Model

The results for the Langmuir Adsorption Isotherm, Temkin Adsorption Isotherm, Flory-Huggins Adsorption Isotherm and Frumkin Adsorption Isotherm at a Temperature of 70^{o}C are shown in Figure 4.33-4.36 respectively. A close observation of the results show that the Experimental results deviated from all the Adsorption Isotherm as evidenced from their low Coefficient of determination values of 86.8%(Langmuir), 43.9% (Temkin), 9.5%(Flory-Huggins) and 76.8% (Frumkin) respectively. Observation similar to those presented here was also reported by (Li et al., 2019; Yang et al., 2019).

Adsorption isotherm for pH 3.15 and Temperature 80^{o}C

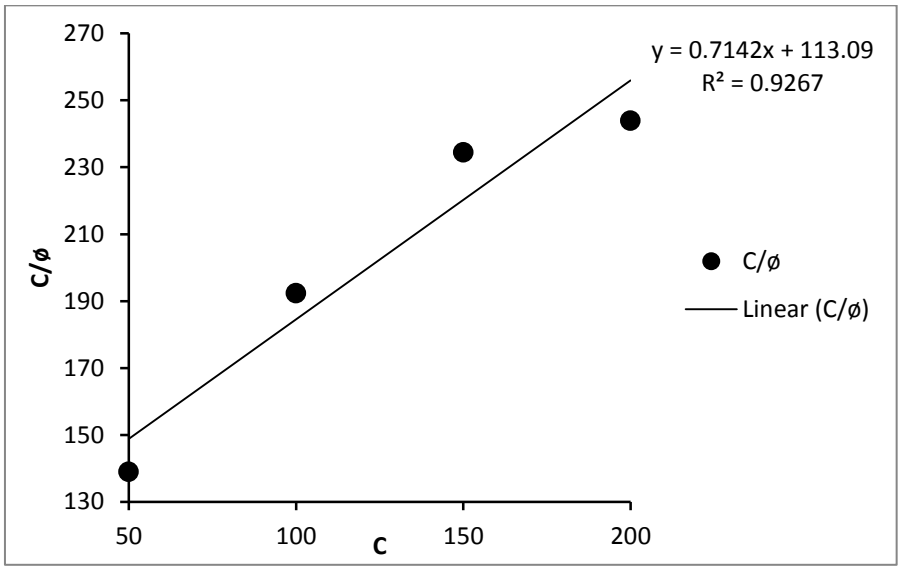

Figure 3.21: Langmuir model

DOI: 10.31695/IJASRE.2020.33938

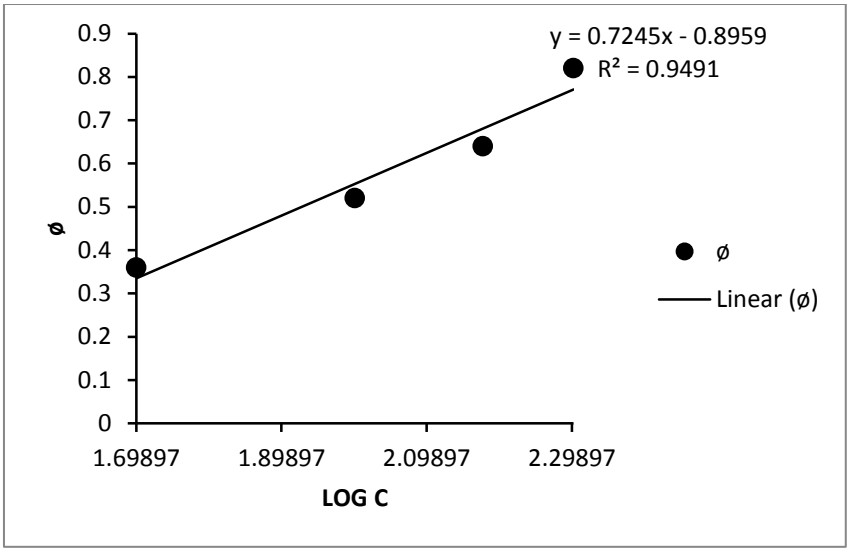

Figure 3.22: Temkin model

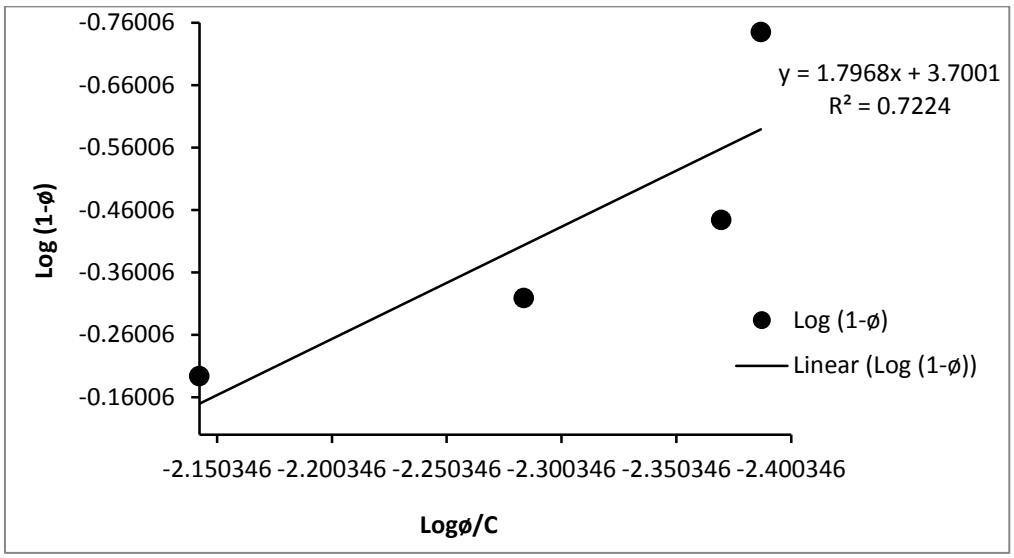

Figure 3.33: Flory-Huggins model

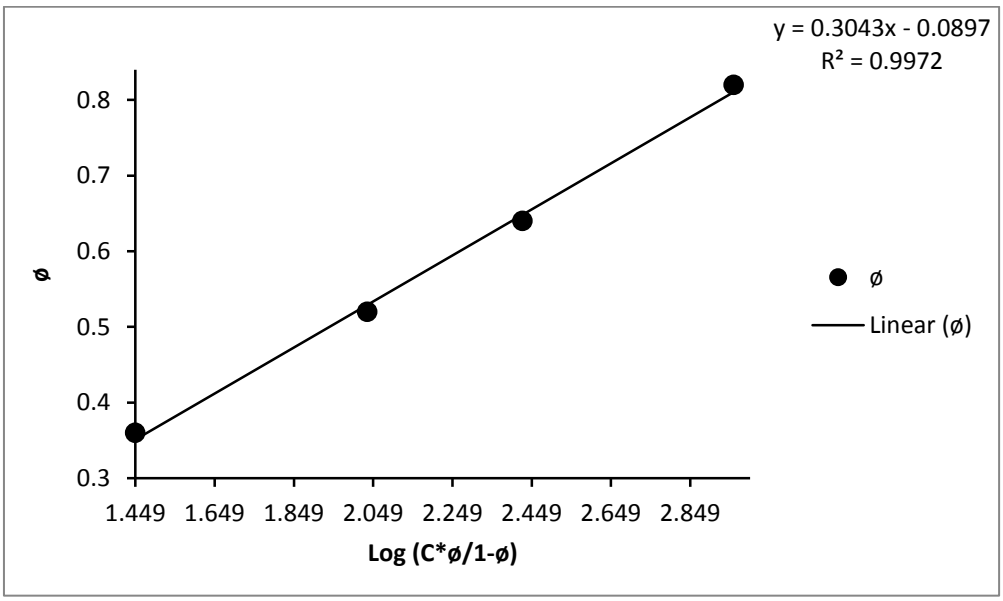

Figure 3.34: Frumkin Model

DOI: 10.31695/IJASRE.2020.33938

3.3 FTIR Analysis

The FTIR was used to identify the types of chemical bonds (Functional groups) present in the Watermelon seed extract. The wavelength of the light absorbed is

Characteristics of the chemical bond as can be seen in the annotated spectrum below (Figure 4.6). By the interpretation of the Infrared absorption spectrum, the Chemical bonds in the Extract were determined (De Spiegelaere et al., 2020; Taheri et al., 2017; Velayi and Norouzbeigi, 2019).

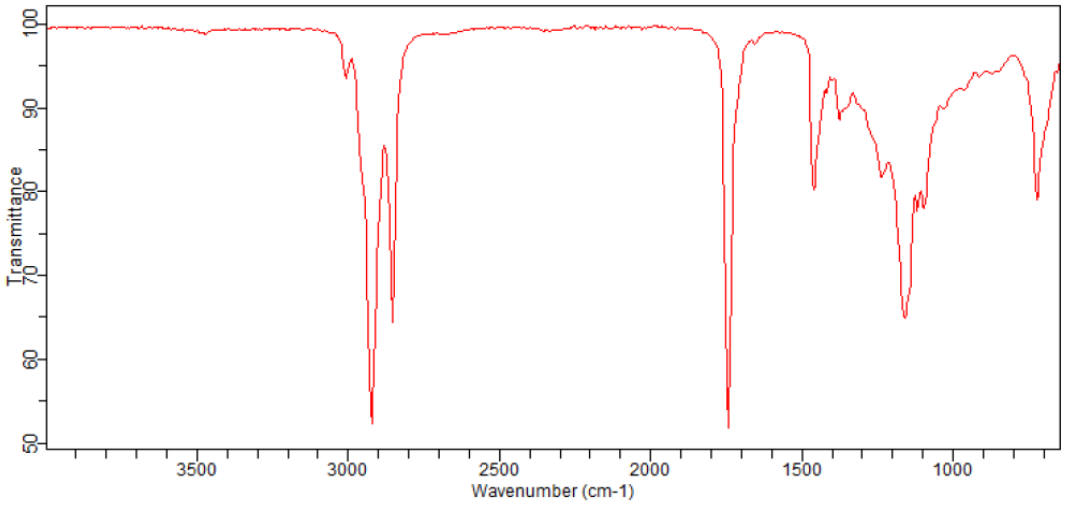

Figure 3.35: FTIR Result for *Citrullus lanatus* Seed Extract

The Fourier Transform Infrared Spectroscopy (FTIR) result is as shown in figure 4.6. From figure 3.35, it should be noted that the functional group of the Watermelon seed extract are represented from 1382cm^{-1} Area of the FTIR result.

Table 3.10: Bond and Wavenumber of the *Citrullus lanatus* Extract.

Bond	Wavenumber (cm^{-1})
R-OH	3385
R-OOH	2929
C-H	2343
C=O	1382
N-H	1622

Source: (Ashokkumar, 2014)

Table 4.1 represents the functional groups and corresponding Wave number of the Watermelon seed extract. Analysis of the Result (Table 4.1) shows that the *Citrullus lanatus* extract was made up of Alcohol, Alcholic Acid, Amine, Ketone etc. These compounds are capable of providing the strong attractive force needed for the Inhibitor Additive to bind to the Metal surface, thus, preventing the spread of corrosion (Li, et al., 2019).

4. CONCLUSION

- From the results obtained, the corrosion rate decreases from 0.57mg/hr to 0.21mg/hr while its Inhibitive efficiency increases with an Inhibitor concentration of 0mg/l to 200mg/l respectively.
- Temperature had two conflicting effect. With a rise in temperature, corrosion rate shows increase and decrease with respect to the solubility limit of Iron Carbonate.
- It was observed that at low pH, the formation of hydrogen ions increases thereby reducing the formation of the protective film on the Coupon which results to an increase in corrosion rate.
- The test sample without inhibitor additive had the lowest activation energy of 4.03Kj/Mol with a further increase of activation energy from 12.65Kj/Mol to 13.75Kj/Mol with Inhibitor concentration of 50ppm to 200ppm.
- From the Adsorption Isotherm tested, the Frumkin Model closely fits the Experimental data at a Temperature of 50^{o}C as evidence from its high Coefficient of determination, R2 value of 99.9%.

REFERENCES

DOI: 10.31695/IJASRE.2020.33938

1. Abdullahi, T., Harun, Z., Othman, M.H.D., Yousuf, A.B., Blaou, A.H.N., Bagaber, S.A., 2020. Effect of Yttrium on the Microstructure and Mechanical Properties of A5083 Secondary Aluminum Alloy.
2. Ademoh, N.A., 2012. Inhibition characteristics of watermelon oil on aluminium in acid and saline water. Assumpt. Univ. J. Technol. AU JT 15, 265–72.
3. Adesina, O.S., Farotade, G.A., Popoola, A.P.I., Oloruntoba, D.T., 2020. INFLUENCE OF CEO2 ADDITION AND SCANNING SPEED ON MICROSTRUCTURE AND TRIBOLOGICAL BEHAVIOR OF LASER-CLAD Ti-Co REINFORCED COATINGS ON Ti-6Al-4V ALLOY. Surf. Rev. Lett. 27, 1950129.
4. Afolabi, A.E., Popoola, O., Popoola, A.P., Aramide, F.O., Oloruntoba, D.T., 2020. Temperature effects on microstructure and mechanical properties of sintered high-entropy equiatomic Ti 20 V 20 Al 20 Fe 20 Cr 20 alloy for aero-gear application. Int. J. Adv. Manuf. Technol. 108, 3563–3570.
5. Akhavan, H., Izadi, M., Mohammadi, I., Shahrabi, T., Ramezanzadeh, B., 2018. The synergistic effect of BTA-Co system on the corrosion inhibition of mild steel in 3.5 wt% NaCl solution. J. Electrochem. Soc. 165, C670.
6. Akinbulumo, O.A., Odejobi, O.J., Odekanle, E.L., 2020. Thermodynamics and adsorption study of the corrosion inhibition of mild steel by Euphorbia heterophylla L. extract in 1.5 M HCl. Results Mater. 5, 100074. https://doi.org/10.1016/j.rinma.2020.100074
7. Al-Haj-Ali, A.M., Jarrah, N.A., Mu'Azu, N.D., Rihan, R.O., 2014. Thermodynamics and kinetics of inhibition of aluminum in hydrochloric acid by date palm leaf extract. J. Appl. Sci. Environ. Manag. 18, 543–551.
8. Ashokumar,S. and Muthukumaran,S.2014. Microstructure, Optical and FTIR studies of Ni, Cu co-doped ZnO nanoparticles by co-precipitation method. Elsevier, 37. 671-678.
9. Cen, H., Cao, J., Chen, Z., Guo, X., 2019. 2-Mercaptobenzothiazole as a corrosion inhibitor for carbon steel in supercritical CO2-H2O condition. Appl. Surf. Sci. 476, 422–434.
10. Chakravarthy, M.P., Mohana, K.N., 2014. Adsorption and Corrosion Inhibition Characteristics of Some Nicotinamide Derivatives on Mild Steel in Hydrochloric Acid Solution. ISRN Corros. 2014, 1–13. https://doi.org/10.1155/2014/687276
11. Chesnokova, M.G., Shalaj, V.V., Kraus, Y.A., Cherkashina, N.V., Mironov, A.Y., 2016. Analysis of corrosion defects on oil pipeline surface using scanning electron microscopy and soil thionic and sulfate-reducing bacteria quantification. Procedia Eng. 152, 247–250.
12. De Spiegelaere, W., Caboor, L., Van Impe, M., Boone, M.N., De Backer, J., Segers, P., Sips, P., 2020. Corrosion casting of the cardiovascular structure in adult zebrafish for analysis by scanning electron microscopy and X-ray microtomography. Anat. Histol. Embryol.
13. Donatus, U., Thompson, G.E., Omotoyinbo, J.A., Alaneme, K.K., Aribo, S., Agbabiaka, O.G., 2017. Corrosion pathways in aluminium alloys. Trans. Nonferrous Met. Soc. China 27, 55–62.
14. Durowaye, S.I., Alabi, A.G.F., Sekunowo, O.I., Bolasodun, B., Rufai, I.O., 2014. Effects of pH Variation on Corrosion of Mild Steel in Bore-hole Water using 1M Sodium Hydroxide Solution. Int. J. Eng. Technol. 4, 7.
15. Fang, H., Nesic, S., Brown, B., Wang, S., Technologies, C., n.d. 06372 - GENERAL CO2 CORROSION IN HIGH SALINITY BRINES 15.
16. Farhadian, A., Rahimi, A., Safaei, N., Shaabani, A., Abdouss, M., Alavi, A., 2020. A theoretical and experimental study of castor oil-based inhibitor for corrosion inhibition of mild steel in acidic medium at elevated temperatures. Corros. Sci. 175, 108871.
17. Fiori-Bimbi, M.V., Alvarez, P.E., Vaca, H., Gervasi, C.A., 2015. Corrosion inhibition of mild steel in HCL solution by pectin. Corros. Sci. 92, 192–199.
18. Go, L.C., Depan, D., Holmes, W.E., Gallo, A., Knierim, K., Bertrand, T., Hernandez, R., 2020. Kinetic and thermodynamic analyses of the corrosion inhibition of synthetic extracellular polymeric substances. PeerJ Mater. Sci. 2, e4. https://doi.org/10.7717/peerj-matsci.4
19. Go, L.C., Holmes, W., Hernandez, R., 2019. Sweet corrosion inhibition on carbon steel using waste activated sludge extract, in: 2019 IEEE Green Technologies Conference (GreenTech). IEEE, pp. 1–4.
20. Gunavathy, N., Murugavel, S.C., 2012. Corrosion Inhibition Studies of Mild Steel in Acid Medium Using *Musa Acuminata* Fruit Peel Extract. E-J. Chem. 9, 487–495. https://doi.org/10.1155/2012/952402
21. Han, P., Chen, C., Li, W., Yu, H., Xu, Y., Ma, L., Zheng, Y., 2018. Synergistic effect of mixing cationic and nonionic surfactants on corrosion inhibition of mild steel in HCl: experimental and theoretical investigations. J. Colloid Interface Sci. 516, 398–406.
22. Hassan, K.H., Khadom, A.A., Kurshed, N.H., 2016. Citrus aurantium leaves extracts as a sustainable corrosion inhibitor of mild steel in sulfuric acid. South Afr. J. Chem. Eng. 22, 1–5.
23. Hribšek, U., n.d. Introduction to corrosion 12.

DOI: 10.31695/IJASRE.2020.33938

24. Ibrahim, T.H., Gomes, E.E., Obot, I.B., Khamis, M., Sabri, M.A., 2017. Mild steel green inhibition by Ficus carica leaves extract under practical field conditions. J. Adhes. Sci. Technol. 31, 2697–2718.
25. Lgaz, H., Salghi, R., Jodeh, S., Hammouti, B., 2017. Effect of clozapine on inhibition of mild steel corrosion in 1.0 M HCl medium. J. Mol. Liq. 225, 271–280.
26. Li, D., Zhang, P., Guo, X., Zhao, X., Xu, Y., 2019. The inhibition of mild steel corrosion in 0.5 M H_2SO_4 solution by radish leaf extract. RSC Adv. 9, 40997–41009. https://doi.org/10.1039/C9RA04218K
27. Loto, R.T., 2018. Surface coverage and corrosion inhibition effect of Rosmarinus officinalis and zinc oxide on the electrochemical performance of low carbon steel in dilute acid solutions. Results Phys. 8, 172–179. https://doi.org/10.1016/j.rinp.2017.12.003
28. Mamedaliev Institute of Petrochemical Processes, National Academy of Sciences of Azerbaijan, AZ1025 Baku, Azerbaijan, Ismayilov, I.T., Abd El-Lateef, H.M., Chemistry Department, Faculty of Science, Sohag University, 82524 Sohag, Egypt, Abbasov, V.M., Mamedaliev Institute of Petrochemical Processes, National Academy of Sciences of Azerbaijan, AZ1025 Baku, Azerbaijan, Efremenko, E.N., Faculty of Chemistry, Lomonosov Moscow State University, 119991, GSP-1, 1-3 Leninskiye Gory, Moscow, Russia, Aliyeva, L.I., Mamedaliev Institute of Petrochemical Processes, National Academy of Sciences of Azerbaijan, AZ1025 Baku, Azerbaijan, Salmanova, Ch.K., Mamedaliev Institute of Petrochemical Processes, National Academy of Sciences of Azerbaijan, AZ1025 Baku, Azerbaijan, 2015. Enhanced corrosion inhibition of mild steel in CO2-saturated solutions containing some novel green surfactants based on cottonseed oil. Int. J. Corros. Scale Inhib. 4, 057–074. https://doi.org/10.17675/2305-6894-2015-4-1-057-074
29. Obot, I.B., Onyeachu, I.B., Umoren, S.A., 2019. Alternative corrosion inhibitor formulation for carbon steel in CO2-saturated brine solution under high turbulent flow condition for use in oil and gas transportation pipelines. Corros. Sci. 159, 108140.
30. Oguntade, T.I., Ita, C.S., Sanmi, O., Oyekunle, D.T., 2020. A Binary Mixture of Sesame And Castor Oil as an Ecofriendly Corrosion Inhibitor of Mild Steel In Crude Oil. Open Chem. Eng. J. 14, 25–35. https://doi.org/10.2174/1874123102014010025
31. Oloruntoba, D.T., Adesina, O.S., Falana, O., Akinluwade, K.J., 2020. Effect of Preheat Treatment on Wear and Corrosion Rates of Copper Electrodeposition on Medium-Carbon Steel. J. Fail. Anal. Prev. 20, 1754–1764.
32. Oluyori, R.T., Alao, A.O., Barnabas, A.A., Shittu, S.A., Omole, S.O., Akinwande, A.A., 2020. effect of heat treatment method on the hardness and corrosion of ductile iron in 3.5% sodium chloride solution. j. doi 6.
33. Onyeachu, I.B., Obot, I.B., Sorour, A.A., Abdul-Rashid, M.I., 2019. Green corrosion inhibitor for oilfield application I: electrochemical assessment of 2-(2-pyridyl) benzimidazole for API X60 steel under sweet environment in NACE brine ID196. Corros. Sci. 150, 183–193.
34. Oyekunle, D.T., Agboola, O., Ayeni, A.O., 2019. Corrosion Inhibitors as Building Evidence for Mild Steel: A Review. J. Phys. Conf. Ser. 1378, 032046. https://doi.org/10.1088/1742-6596/1378/3/032046
35. Palacios, C.A., Shadley, J.R., 1991. Characteristics of corrosion scales on steels in a CO2-saturated NaCl brine. Corrosion 47, 122–127.
36. Palumbo, G., Górny, M., Banaś, J., 2019. Corrosion Inhibition of Pipeline Carbon Steel (N80) in CO2-Saturated Chloride (0.5 M of KCl) Solution Using Gum Arabic as a Possible Environmentally Friendly Corrosion Inhibitor for Shale Gas Industry. J. Mater. Eng. Perform. 28, 6458–6470. https://doi.org/10.1007/s11665-019-04379-3
37. A., Linke, B., Kranzmann, A., 2011. Corrosion behaviour of pipe steels exposed for 2 years to CO2 -saturated saline aquifer environment similar to the CCS-site Ketzin, Germany. Energy Procedia 4, 5122–5129. https://doi.org/10.1016/j.egypro.2011.02.488
38. Rajendrachari, S., 2018. Effect of sintering temperature on the pitting corrosion of ball milled duplex stainless steel by using linear sweep voltammetry. Anal. Bioanal. Electrochem. 10, 349–361.
39. Rivera-Grau, L.M., Casales, M., Regla, I., Ortega-Toledo, D., Cuervo, D., Asencio, J., Gonzalez-Rodriguez, J., Martine-Gomez, L., 2012. Corrosion inhibition by a coconut oil modified imidazoline for carbon steel under the combined effect of CO 2 and H 2 S. Int J Electrochem Sci 7, 12610–12620.
40. Salinas-Solano, G., Porcayo-Calderon, J., de la Escalera, L.M., Canto, J., Casales-Diaz, M., Sotelo-Mazon, O., Henao, J., Martinez-Gomez, L., 2018. Development and evaluation of a green corrosion inhibitor based on rice bran oil obtained from agro-industrial waste. Ind. Crops Prod. 119, 111–124.
41. Singh, A., Lin, Y., Liu, W., Ebenso, E.E., Pan, J., 2013. Extract of Momordica charantia (Karela) Seeds as Corrosion Inhibitor for P110SS Steel in Co2 Saturated 3.5% NaCl Solution. Int J Electrochem Sci 8, 10.
42. Sotelo-Mazon, O., Valdez, S., Porcayo-Calderon, J., Henao, J., Cuevas-Arteaga, C., Poblano-Salas, C.A., Martinez-Gomez, L., 2020. Evaluation of Corrosion Inhibition of 1018 Carbon Steel using an Avocado Oil-Based Green Corrosion Inhibitor. Prot. Met. Phys. Chem. Surf.

DOI: 10.31695/IJASRE.2020.33938

43. Souza, A.V., da Rocha, J.C., Gomes, J.P., Palermo, L.C., Mansur, C.R., 2020. Development and application of a passion fruit seed oil microemulsion as corrosion inhibitor of P110 carbon steel in CO2-saturated brine. Colloids Surf. Physicochem. Eng. Asp. 124934.
44. Taheri, M., Naderi, R., Saremi, M., Mahdavian, M., 2017. Development of an ecofriendly silane sol-gel coating with zinc acetylacetonate corrosion inhibitor for active protection of mild steel in sodium chloride solution. J. Sol-Gel Sci. Technol. 81, 154–166.
45. Tariq Saeed, M., Saleem, M., Niyazi, A.H., Al-Shamrani, F.A., Jazzar, N.A., Ali, M., 2020. Carrot (Daucus Carota L.) Peels Extract as an Herbal Corrosion Inhibitor for Mild Steel in 1M HCl Solution. Mod. Appl. Sci. 14, 97. https://doi.org/10.5539/mas.v14n2p97
46. Tasić, Ž.Z., Mihajlović, M.B.P., Radovanović, M.B., Simonović, A.T., Antonijević, M.M., 2018. Cephradine as corrosion inhibitor for copper in 0.9% NaCl solution. J. Mol. Struct. 1159, 46–54.
47. Velayi, E., Norouzbeigi, R., 2019. Single-step prepared hybrid ZnO/CuO nanopowders for water repellent and corrosion resistant coatings. Ceram. Int. 45, 16864–16872.
48. Veneranda, M., Costantini, I., de Vallejuelo, S.F.-O., Garcia, L., García, I., Castro, K., Azkarate, A., Madariaga, J.M., 2016. Study of corrosion in archaeological gilded irons by Raman imaging and a coupled scanning electron microscope–Raman system. Philos. Trans. R. Soc. Math. Phys. Eng. Sci. 374, 20160046.
49. Xu, X., Singh, A., Sun, Z., Ansari, K.R., Lin, Y., 2017. Theoretical, thermodynamic and electrochemical analysis of biotin drug as an impending corrosion inhibitor for mild steel in 15% hydrochloric acid. R. Soc. Open Sci. 4, 170933. https://doi.org/10.1098/rsos.170933
50. Yang, D., Ye, Y., Su, Y., Liu, S., Gong, D., Zhao, H., 2019. Functionalization of citric acid-based carbon dots by imidazole toward novel green corrosion inhibitor for carbon steel. J. Clean. Prod. 229, 180–192.

DOI: 10.31695/IJASRE.2020.33938